Iranian Journal of Medical Physics

ijmp.mums.ac.ir

Comparative Analysis of Gamma-Ray Shielding in Glass Systems with Pb/Bi Heavy Elements

Mohammadreza Alipoor[1], Mahdi Eshghi [1*]

1. Department of Physics, Faculty of Basic Sciences, Imam Hossein University, Tehran, Iran

ARTICLE INFO

Article type:
Original Paper

Article history:
Received: May 01, 2025
Accepted: Aug 04, 2025

Keywords:
Shielding
Geant4
Glass
Gamma-ray
Radiation Protection

ABSTRACT

Introduction: The development of effective, eco-friendly radiation shielding materials is critical for medical and nuclear applications. This research investigates the effect of bismuth oxide (Bi_2O_3) content on the gamma-ray attenuation properties of $PbO–Al_2O_3–B_2O_3–SiO_2–Bi_2O_3$ glasses.

Material and Methods: Six distinct glass compositions, characterized by varying mole fractions of Bi_2O_3, were meticulously selected for this study. The mass attenuation coefficients (MAC) and linear attenuation coefficients (LAC) were computed utilizing the Geant4 Monte Carlo simulation toolkit and subsequently validated against the Phy-X/PSD computational software. The half-value layer (HVL), tenth-value layer (TVL), and effective atomic number (Z_{eff}) were derived across a gamma-ray energy spectrum ranging from 0.015 to 10 MeV.

Results: Excellent agreement was observed between Geant4 and Phy-X results (relative error < 2%). The LAC increased with Bi_2O_3 content, particularly at low energies (< 0.3 MeV), where sample S-6 (highest Bi_2O_3) exhibited the highest attenuation. HVL and TVL increased with photon energy but decreased with higher Bi_2O_3 concentration, confirming enhanced shielding efficiency. S-6 displayed the lowest TVL, indicating superior performance. Z_{eff} varied significantly with composition and energy, reaching a minimum near 2 MeV for all samples. All glasses showed shielding capabilities comparable to or better than conventional glass shields.

Conclusion: Increasing Bi_2O_3 content substantially improves gamma-ray shielding in lead-bismuth borosilicate glasses, especially at low energies. These glasses are promising candidates for radiation protection applications.

►*Please cite this article as:*
Alipoor MR, Eshghi M. Comparative Analysis of Gamma-Ray Shielding in in Glass Systems with Pb/Bi Heavy Elements. Iran J Med Phys 2025; 22 (5): 305-320. 10.22038/ijmp.2025.88399.2556.

Introduction

Radioactive substances possess the potential to exert considerable influences on both human health and ecological systems. Prolonged exposure to elevated levels of radioactive radiation may culminate in radiation contamination, manifesting symptoms such as nausea, emesis, lethargy, and immunocompromised states [1, 2]. The interplay between ionizing radiation and cellular structures may precipitate damage to cellular and genetic components, with a pronounced effect on deoxyribonucleic acid. Such cellular impairment may lead to either cellular apoptosis or deleterious alterations within the cell, including mutations, thereby heightening the propensity for malignancies such as thyroid carcinoma, leukemia, and various solid tumors. Furthermore, the incidence of congenital disorders and genetic anomalies escalates with increased doses of ionizing radiation, as radiation possesses the ability to alter genetic material, thereby impacting successive generations [3]. The usage of radiation shielding materials represents a paramount strategy for mitigating ionizing radiation exposure. Specific compounds or structural designs, identified as radiation shields, are capable of absorbing or attenuating ionizing radiation, including gamma rays, X-rays, or high-energy particles [4, 5]. The principal objective of such shielding materials is always to establish a secure environment for personnel engaged in radiological activities within nuclear facilities. To achieve this objective, various protective materials ,including polymers, concrete, glass, alloys, and stones, are employed [6, 9]. The efficacy of the shielding material is contingent upon various factors, including its composition, thickness, atomic number, and density; thus, the choice of an appropriate shielding material necessitates consideration of multiple criteria. The radiation absorption or attenuation capabilities exhibited by diverse materials may exhibit significant variability [10, 11]. Glass has emerged as a contemporary technological advancement owing to its application in engineering designs and innovations over recent decades. Given the direct correlation involving the chemical composition of glasses and their overall attributes, the performance of a specific glass can either be constrained or enhanced based on its compositional

*Corresponding Author: Tel: +98-09905404390; Email: mohamadrezaalipoor1997@gmail.com

makeup. Consequently, distinct glass systems are optimized for functionalities relative to others [12, 13]. Protective glass is integral in a multitude of settings, serving to safeguard against potentially deleterious radiation, intense illumination, or hazardous substances. The design and materials employed in these protective glasses must be meticulously engineered to deliver requisite protection while maintaining visibility and comfort [14-18]. Considering the distinctive characteristics of silicate glasses, researchers are persistently exploring methodologies to augment the properties of silicate glass and to identify novel compounds or techniques to enhance its flexibility, transparency, and environmental compatibility [19-22]. As a reinforcing agent, bismuth is acknowledged as one of nature's most benign elements. Additionally, Bi_2O_3 is inclined to engage in network formation and contribute to the modification of glass systems through appropriate arrangement within the borate-based glass framework [23, 24]. The incorporation of higher valence oxide Bi_2O_3 can induce various structural modifications within the glass system. Primarily, Bi^{3+} ions facilitate structural alterations; however, upon the introduction of Bi^{3+} ions exceeding 45 mol%, they are able to serve effectively as a network supplier [24, 25]. B_3O_4, diborate B_3O_8, and tri-borate B_3O_7 coexist alongside other complex groups. In the context of the silicate glasses currently under investigation, the glass network is modified with bismuth oxide Bi_2O_3 due to its extensive applicability across diverse domains [26]. In previous studies, numerous investigations have been performed on glasses incorporating heavy metal oxides (HMO) such as Pb_3O_4, Bi_2O_3, WO_3, and Y_2O_3, revealing an enhancement in their desirable properties for absorbing and attenuating radiation. Contemporary scientific discourse has embraced the paradigm of modifying the attributes of materials at both atomic and molecular dimensions to engender superior protective characteristics which are effective, stable, and flexible [27, 28]. Owing to its amorphous architecture and its aptitude for doping with various elements, glass is regarded as a promising substrate for the advancement of radiation shielding technologies. Empirical evidence has demonstrated that the incorporation of heavy elements can augment the absorption capacity of ionizing radiation, attributable to the influence of high atomic numbers, as seen with elements such as bismuth. The density, mechanical robustness, and optical clarity of glass may be altered by the introduction of appropriate reinforcements, yielding significant advantages through the tailored development of radiation shielding applications that meet specific requirement [29, 30]. This research endeavors to elucidate the effects of Bi_2O_3 supplementation in a glass matrix comprised of PbO-Al_2O_3-B_2O_3-SiO_2 on its efficacy in radiation blockage and to analyze how varying concentrations of Bi_2O_3 influence its radiation shielding capabilities. The development of specialized radiation shielding materials with enhanced performance and additional advantageous attributes underscores the significance of this inquiry, as the outcomes could pave the way in which for the innovation of glass-based products pertinent to radiology, industrial applications, and the management of nuclear waste. The theoretical assessment of the radiation shielding properties of diverse glass formulations has been substantiated as a means of expediting the identification of novel materials and ameliorating their performance through computational methodologies such as Geant4, thereby obviating the necessity for time-consuming experimental resources.

Materials and Methods

In the present investigation centered on the radiation attenuation characteristics of PbO-Al_2O_3-B_2O_3-SiO_2-Bi_2O_3 glass composites, the glasses formulated by Waly et al. [31] were meticulously chosen for analysis: To more evaluate the radiation shielding efficacy of the selected glass compositions, the Geant4 simulation toolkit was employed to compute various shielding parameters across the energy spectral range of 0.015 to 10 MeV. This energy range was selected because of its association with well-established radioactive sources that find extensive applications in medical imaging, radiopharmaceuticals, industrial radiography, and nuclear research, among other disciplines. Geant4 represents a pivotal software resource for professionals engaged in radiation physics, as its primary purpose is to furnish precise data regarding the interactions of photons with designated materials. Concerning the advancement of innovative radiation shielding substances, a comprehensive assessment of the fundamental parameters that characterize the attenuation of gamma radiation is of paramount importance. All these values serve a distinct purpose in elucidating how various materials engage with various photon types and offer valuable insights into their efficacy in diminishing photon intensity.

Geant4 toolkit

Investigations in particle and beam physics encompass intricate processes, rendering it advantageous to conduct simulation modeling before the commencement of experimental procedures. In the context of radiation shielding examinations, this significantly streamlines the propagation of radiation events through shielding materials, supplies essential information to the user, and informs the development of novel materials. In the present study, we utilized the Geant4 framework to simulate the transport of photons with a particular focus on the energy range of 0.015 to 10 MeV. The primary aim of the simulation was to determine the linear attenuation coefficients of the two composite materials, from which further shielding parameters such as half-value layer and tenth-value layer may be extrapolated. The simulation was carried

out using a singular cubic box with dimensions measuring 5 cm, made of a homogeneous material. The photon interaction cross sections were calculated utilizing the G4EMStandardPhysics physics list within the Geant4 toolkit, specifically to evaluate the attenuation behavior of gamma and X-ray photons as they pass through the material under study. In these simulations, Geant4 stochastically models the full cascade of particle interactions, including key quantities such as secondary particles energy, the count of transmitted photons, and the amount of photons removed from the beam due to attenuation processes (e.g., photoelectric absorption, Compton scattering, and pair production). To maintain simulation fidelity and computational efficiency, a transportation cut-off threshold of 0.1 mm was uniformly applied to all secondary particles. This cut-off defines the minimum step length a secondary particle must travel before itis explicitly tracked; particles with ranges below this threshold deposit their energy locally, which helps preserve accuracy without excessive computational overhead. Each simulation run was configured to emit 10^7 primary photons from a monoenergetic point source. This large amount of incident particles was chosen deliberately to ensure that the statistical uncertainty in all measured quantities—such as transmission fractions and attenuation coefficient remained at or below 1.5%. By simulating a high-statistics ensemble of events, random fluctuations were significantly reduced, thereby enhancing the robustness and reliability of the results and strengthening the overall scientific validity of the conclusions drawn from the data [32, 33]. The configuration of the Geant4 simulation employed in this study is illustrated in Figure 1.

Phy-X/PSD Program

The Phy-X/PSD software is a widely used computational tool designed to evaluate an extensive set of radiation shielding parameters over a broad photon energy range. To perform these calculations, the user must input two essential material properties: the chemical composition expressed as weight fractions and the physical density (in g/cm³). The program operates effectively across photon energies spanning from 0.015 MeV to 10 MeV, which covers the most relevant energy range encountered in diagnostic radiology, nuclear medicine, industrial radiography, and radiation protection scenarios.

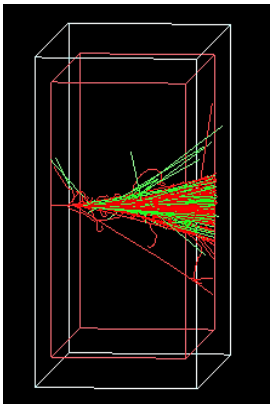

Figure 1. Schematic of configuration of shielding in Geant4 tool

The reliability and accuracy of Phy-X/PSD has been well established in the literature [34], and it is commonly employed by researchers as a benchmarking tool to validate both experimental measurements and Monte Carlo simulation outcomes. When results from independent simulations (e.g., using Geant4 or MCNP) show close agreement—typically with small deviations (<2–3%)—with those generated by Phy-X/PSD, this consistency serves as strong evidence of the validity and credibility of the simulated data [35, 36].

Studied Radiation Shielding Parameters

The determination of the Linear attenuation coefficient (LAC) is the initial phase in assessing the material's effectiveness for shielding. The LAC can be ascertained through the application of Beer-Lambert's law [37]:

$$LAC = -\frac{1}{x}\ln(\frac{I}{I_0}) \quad (1)$$

where ρ is a density of material. The theoretical MAC values for the designated samples were computed utilizing the Phy-x software. Furthermore, the relative deviation (RD%) between the Geant4 toolkit and theoretical MAC values at the examined photon energies is delineated in Table 2. The RD% is determined in accordance with the provided expression [37].

Table 1. Chemical composition and Weight fraction of elements for S1-S6 glass evaluated

Glass Code	Density	Mole fraction of compounds					Wi: Weight Fraction of Elements					
	g/cm³	% mol					Wi%					
		PbO	Al_2O_3	B_2O_3	SiO_2	Bi_2O_3	Pb	O	Al	Bi	B	Si
S1	3.6125	0.1	---	0.2	0.65	0.05	0.2101	0.3489	---	0.2120	0.0439	0.1852
S2	4.3765	0.25	0.10	0.65	---	---	0.4656	0.3595	0.1263	---	0.0485	---
S3	5.513	0.40	0.10	0.10	0.40	---	0.6352	0.2207	0.0414	---	0.0166	0.0861
S4	6.22	0.50	0.10	---	0.40	---	0.7104	0.1755	0.0370	---	---	0.0770
S5	7.801	0.30	---	0.20	---	0.50	0.1980	0.1223	---	0.6658	0.0138	---
S6	8.4955	0.35	---	---	0.10	0.55	0.2130	0.1034	---	0.6753	---	0.0083

Table 2. Mass attenuation coefficients of S1-S6 glass evaluated

Photon Energy (MeV)	S1			S2			S3			S4			S5			S6		
	Phy- X	Geant4	RD%	Phy- X	Geant4	RD%	Phy-X	Geant4	RD%	Phy- X	Geant4	RD%	Phy- X	Geant4	RD%	Phy- X	Geant4	RD%
0.015	50.6	49.985	1.23	53.060	52.917	0.27	72.510	72.259	0.35	80.680	80.471	0.26	99.53	99.415	0.12	102.3	102.22	0.07
0.02	38.27	37.69	1.54	40.730	40.564	0.41	55.590	55.311	0.50	61.990	61.728	0.42	76.81	76.495	0.41	78.97	78.645	0.41
0.04	6.415	6.331	1.32	6.829	6.813	0.23	9.266	9.236	0.32	10.320	10.298	0.21	12.83	12.804	0.20	13.19	13.158	0.24
0.05	3.629	3.574	1.55	3.860	3.841	0.50	5.211	5.181	0.58	5.798	5.769	0.50	7.199	7.166	0.46	7.396	7.3622	0.46
0.06	2.297	2.256	1.81	2.439	2.421	0.76	3.273	3.244	0.89	3.635	3.606	0.81	4.504	4.469	0.78	4.625	4.5896	0.77
0.08	1.149	1.127	1.91	1.215	1.192	1.92	1.604	1.571	2.10	1.773	1.738	2.04	2.181	2.1592	1.01	2.237	2.1988	1.74
0.1	2.477	2.443	1.40	2.665	2.663	0.09	3.584	3.578	0.17	3.990	3.986	0.10	4.94	4.9221	0.36	5.074	5.0559	0.36
0.15	0.945	0.931	1.46	1.009	1.005	0.38	1.330	1.324	0.48	1.471	1.466	0.37	1.804	1.7959	0.45	1.851	1.8425	0.46
0.2	0.501	0.494	1.32	0.530	0.528	0.39	0.680	0.677	0.44	0.746	0.743	0.36	0.9025	0.8989	0.40	0.9244	0.9208	0.40
0.5	0.119	0.119	0.17	0.121	0.121	0.22	0.134	0.134	0.16	0.140	0.140	0.17	0.154	0.1539	0.07	0.1559	0.1558	0.04
0.6	0.100	0.100	0.11	0.100	0.101	0.33	0.109	0.109	0.21	0.112	0.112	0.23	0.1206	0.1208	0.18	0.1218	0.122	0.16
0.8	0.079	0.079	0.48	0.078	0.079	0.61	0.082	0.082	0.56	0.083	0.084	0.57	0.0873	0.0877	0.50	0.0878	0.0883	0.50
1.17	0.060	0.060	0.40	0.060	0.060	0.44	0.061	0.061	0.48	0.061	0.061	0.49	0.062	0.0623	0.48	0.0621	0.0624	0.48
1.33	0.056	0.056	0.37	0.055	0.055	0.42	0.056	0.056	0.46	0.056	0.056	0.47	0.0565	0.0568	0.45	0.0566	0.0568	0.46
1.5	0.052	0.052	0.35	0.051	0.052	0.38	0.052	0.052	0.42	0.052	0.052	0.44	0.0525	0.0528	0.43	0.0526	0.0528	0.43
2	0.045	0.045	0.12	0.045	0.045	0.09	0.045	0.045	0.07	0.046	0.046	0.07	0.0462	0.0461	0.11	0.0463	0.0462	0.11
3	0.039	0.039	0.51	0.039	0.038	0.41	0.040	0.040	0.40	0.041	0.040	0.39	0.0417	0.0416	0.38	0.0419	0.0418	0.38
4	0.036	0.036	0.36	0.036	0.036	0.19	0.038	0.038	0.1	0.039	0.039	0.03	0.0407	0.0408	0.10	0.0411	0.0411	0.10
5	0.034	0.034	0.11	0.034	0.034	0.16	0.037	0.038	0.31	0.039	0.039	0.43	0.0409	0.0412	0.63	0.0414	0.0416	0.64
6	0.034	0.034	0.13	0.034	0.034	0.46	0.037	0.038	0.67	0.039	0.039	0.79	0.0417	0.0421	1.05	0.0422	0.0426	1.06
8	0.033	0.033	0.75	0.034	0.034	0.84	0.038	0.039	1.04	0.040	0.041	1.19	0.0438	0.0444	1.44	0.0444	0.0451	1.48
10	0.034	0.034	0.78	0.034	0.034	0.86	0.040	0.040	1.03	0.042	0.042	1.16	0.0461	0.0468	1.41	0.0469	0.0476	1.43

$$RD\% = \frac{MAC_{Phy-x} - MAC_{Geant4}}{MAC_{Phy-x}} \quad (3)$$

HVL represents a vital parameter in the formulation of effective radiation-shielding material. It is quantitatively defined as the thickness of the absorber required reducing the incident radiation on the material to 50% of its initial intensity and is calculated through the equation provided. Additionally, the thickness at which the intensity of gamma-ray photons transmitted through the material diminishes to one-tenth of its initial value is referred to as the Tenth value layer, which is articulated by the equation (4) [37].

$$HVL = \frac{\ln 2}{LAC}, \qquad TVL = \frac{\ln 10}{LAC} \quad (4)$$

The role of the chemical composition of a shielding material is consistently articulated through the effective atomic number (Z_{eff}), and its variability with energy can be employed to investigate the relative changes in photon absorption phenomena across different shielding materials. The effective electron density (N_{eff}), quantified in electrons per gram, which delineates the number of electrons per unit mass of the material, is derived from the calculated Z_{eff} in accordance with the stipulated equation [37].

$$Z_{eff} = \frac{\sum_i f_i A_i (MAC)_i}{\sum_i f_i \frac{A_i}{Z_i} (MAC)_i}, \qquad N_{eff} = \frac{N_A Z_{eff}}{\sum_i f_i A_i} \quad (5)$$

In this equation, f_i and A_i denote the mean atomic mass of the sample, while N_A signifies Avogadro's number. A pivotal parameter considered in the design of a radiation shielding medium is the buildup factor (BF). BFs are classified into two categories: the energy absorption buildup factor (EABF) and the exposure buildup factor (EBF). BFs were determined through the implementation of the Geometrical Progression (G-P) fitting methodology across energy ranges extending from 0.015 to 10 MeV [37].

B (E, X) =1+((b-1)/(K-1)) (K^x-1) for K≠1

B (E, X) =1+(b-1) X for K=1

$$K(E,X) = CX^a + d\frac{\tanh\left(\frac{X}{X_K}-2\right)-\tanh(-2)}{1-\tanh(-2)} \quad \text{for } x \leq 40mfp \quad (6)$$

where K(E, X) denotes the photon dose multiplication factor, which is derived using: where x represents the mean free path that spans from 1 to 40 mfp ($1 \leq x \leq 40$).

Results

In the present investigation, a thorough examination of the high-concentration heavy metal oxide incorporated into the PbO-Al_2O_3-B_2O_3-SiO_2-Bi_2O_3 (where HMO = PbO, Bi_2O_3) system was conducted with respect to their overall gamma-ray attenuation capabilities. The physical characteristics of the PbO-Al_2O_3-B_2O_3-SiO_2-Bi_2O_3 glass compositions exhibited density values of 3.6125, 4.3765, 5.513, 6.22, 7.801, and 8.4955 g/cm^3, corresponding to varied concentrations of PbO (10%, 25%, 40%, 50%, 30%, and 35% mol), Al_2O_3 (0%, 10%, 10%, 0%, 20%, and 0% mol), B_2O_3 (20%, 65%, 10%, 0%, 20%, and 0% mol), SiO_2 (65%, 0%, 40%, 40%, 0%, and 10% mol), and Bi_2O_3 (5%, 0%, 0%, 0%, 50%, and 55% mol) within the glass matrix. A total of six distinct glass samples, designated as S1 through S6, were categorized based on the type of HMO present within their structural framework. Understanding the chemical and physical properties of diverse materials is crucial for multiple reasons; primarily, it facilitates the identification and categorization of materials. Furthermore, it empowers predictions regarding the behavior of materials and their interactions with other substances across a variety of contexts. Currently, the physical parameters, including density and molar volume of the glasses, are delineated in Table 1. The correlation between average molecular weight is illustrated in Figure 2.

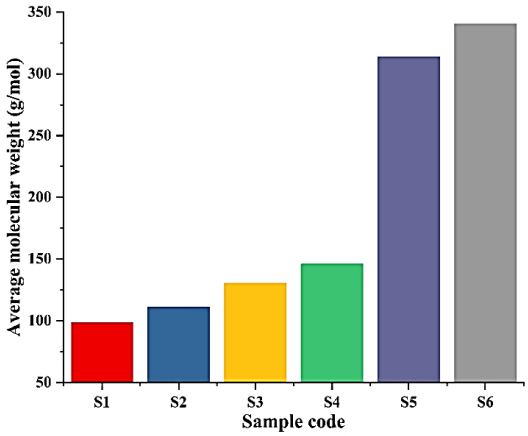

Figure 2. Average molecular weight (g/mol) for S1 to S6 selected glass systems

Figure 2 elucidates the relationship between the molar volume of the heavy metal oxide incorporated into the selected glass samples. It is noteworthy that the molar volume exhibits an increase concomitant with the augmentation of Bi_2O_3 content; this phenomenon aligns with previous findings, which indicated that such increases resulted in the densification of the glass compounds, potentially attributed to novel arrangements within their fundamental structural units. Additionally, the increase in molar volume suggests that the inclusion of Bi_2O_3 leads to an expansion of the glass network. It is distinctly observable that the densities of the HMO-reinforced glass range from 3.61 g/cm^3 to 7.8 g/cm^3. Therefore, it can be asserted that the contribution of Bi_2O_3 has augmented the material density to a greater extent than that of PbO, particularly concerning their HMO configurations, as vividly depicted in Figure 2.

To conduct a comprehensive assessment of the radiation shielding properties of the glasses, it is essential to compute the fundamental parameters that characterize the attenuation of gamma radiation. The initial step involves the verification of the computed values to ensure their precision. This validation procedure entailed a

comparative analysis employing the Geant4 toolkit alongside theoretical results produced via the Phy-X software. The results delineated in Table 2 demonstrate that the relative difference generally diminishes with increasing photon energy. As indicated in Table 2, the calculated values for MAC surpassed the theoretical results obtained from Phy-X/PSD. This divergence can be attributed to the electromagnetic models implemented within Geant4, which proficiently transport photons with high accuracy and yield results of exceptional sensitivity. The relative difference between the computed and theoretical MAC values ranges from 0.228% to 2%. These RD% values signify that Geant4 and Phy-X/PSD exhibit a commendable degree of concordance.

The mass attenuation coefficient (MAC) serves as an essential metric elucidating the capacity of a material to absorb gamma photons. For materials exhibiting superior protective capabilities against gamma photons, it is imperative that the MAC assumes a higher value. The results obtained for the heavy metal oxide glass under investigation are presented in Figure 2. The figure illustrates that the MAC is influenced by both the photon energy and the chemical composition of the glass analyzed. Furthermore, this figure indicates that the MAC values are closely aligned, attributable to the analogous chemical makeup and structural characteristics of the evaluated glass. The samples S5 and S6 exhibited marginally elevated mass attenuation coefficient values compared to the other samples under examination, likely due to the increased concentration of bismuth oxide in sample S6, whereas samples S2 to S5 lack bismuth oxide. Bismuth oxide (molecular weight = 465.959 g/mol) represents the heaviest molecular component within the glass matrix, and elements with higher atomic numbers typically enhance mass attenuation coefficient values. Figure 3 illustrates the variation in the MAC in relation to both partial and total photon interactions. This figure reveals that different photon interactions predominate across varying energy ranges. The photoelectric interaction is the most significant within the extremely low energy spectrum. The phenomena associated with the photoelectric effect (PE), Compton scattering (CS), and pair production (PP) can be delineated through the interactions of photons with the chosen samples. It is apparent that there exists a triad of photon energy ranges: the initial energy band ($E < 1500$ keV), the intermediate energy band (1500 keV $< E < 5000$ keV), and the final energy band (5000 keV $< E$). Within the first energy segment, the results for the MAC of the selected glasses demonstrate a steep decline with the rise in photon energy, characterized by significant peaks attributable to the photoelectric effect occurring around the L3, L2, L1, and K-edges absorption of the bismuth element (at 0.01341, 0.01571, 0.0163875, and 0.9052 MeV, respectively), as well as the L3, L2, L1, and K-edges absorption of the lead element (at 0.01586, 0.0152, 0.013035, and 0.880045 MeV, respectively). The MAC values diminish to below 5 (cm^2/g) as the photon energy ascends to 100 keV. As the photon energy escalates from 100 keV to 1 MeV, the rate of decline in MAC becomes markedly sluggish. This phenomenon arises from the fact that the interaction cross section exhibits an inverse relationship with energy within the Compton scattering domain. Additionally, it is inferred that pair production within the nuclear field initiates when photon energy surpasses 1.02 MeV, with the probability of occurrence augmenting as energy increases, ultimately reaching a plateau at elevated energy levels.

The LAC of the glasses serves as a pivotal parameter within the realm of gamma-ray shielding, as it is subject to various influences, including the radiation energy, the chemical composition of the material, and its density. Glass samples exhibiting elevated LAC values are advantageous for practical applications, as an increased LAC denotes enhanced properties for radiation shielding. The LAC for the glasses can be enhanced through the incorporation of heavy metal oxides (e.g., Bi_2O_3 and PbO utilized in this investigation). Figure 4 illustrates the LAC for the selected glass samples at specific energy levels, with the data indicating that the LAC exhibits significant variations across all glasses. At lower energy levels, sample S6 demonstrates higher LAC values relative to samples S1 through S5. As the energy escalates, the LAC for all chosen samples generally exhibits a decrease. This phenomenon can be attributed to the interaction between gamma photons and the atomic structure of these glasses. Within the low-energy range of 0.015 to 0.2 MeV, all glass samples reveal a comparatively steep decline in the LAC as energy increases, suggesting a more pronounced reduction in shielding efficacy at elevated energy levels.

In the energy interval of 0.2 to 3 MeV, the reduction in LAC values appears to exhibit a deceleration, indicating a more gradual decline in shielding effectiveness. For energies exceeding 3 MeV, the rate of decrease in the LAC further stabilizes, implying that the shielding efficacy of the glasses becomes increasingly consistent at high-energy levels. It was also observed that the LAC is contingent upon the density of the glasses. Sample S6 exhibits the highest LAC, while the lowest LAC was recorded for sample S1, with the observed disparity attributed to the differing concentrations of Bi_2O_3 in the glass compositions. Sample S6, which contains a greater proportion of Bi_2O_3 compared to sample S1, consistently exhibits higher LAC values across all selected energy levels.

To assess the efficacy of radiation shielding provided, Figure 5 presents a comparative analysis of the LAC values at 0.662 MeV for these materials in relation to previously reported lead-glasses [38].

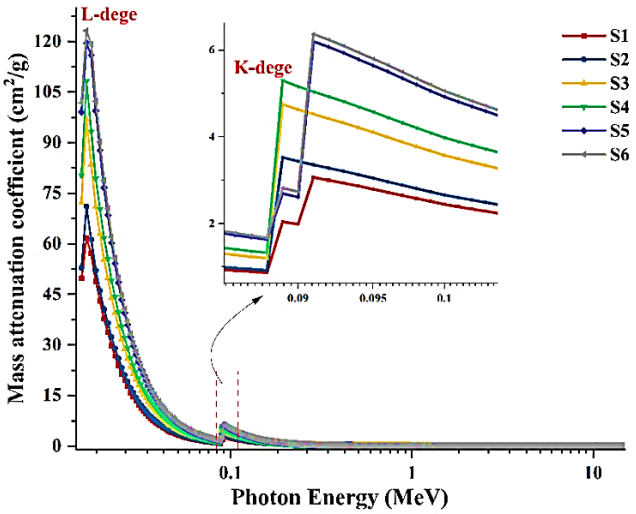

Figure 3. Mass attenuation coefficient for S1 to S6 selected glass systems

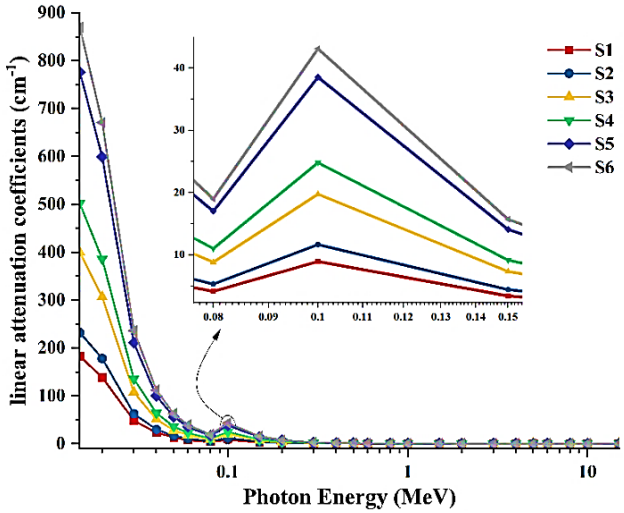

Figure 4. Linear attenuation coefficient for S1 to S6 selected glass systems

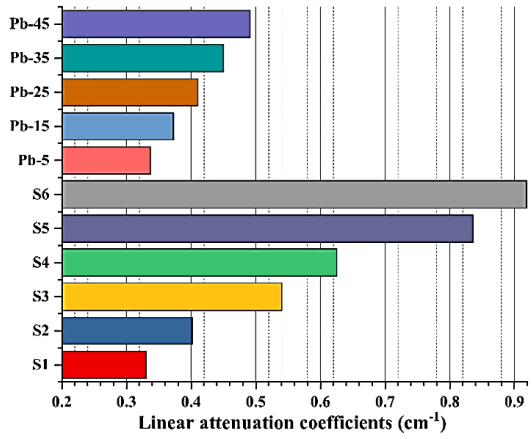

Figure 5. Comparison of linear attenuation coefficient for selected glass samples

The LAC values for the selected glasses at 0.662 MeV are recorded as 0.3302, 0.4014, 0.5401, 0.6255, 0.8364, and 0.9186 cm^{-1} for glasses S1 through S6, respectively. These values surpass those reported for Pb-glasses with 5, 15, 25, 35, and 45 mole percent concentrations, which are 0.3368, 0.3728, 0.4109, 0.4503, and 0.4914 cm^{-1}, respectively. Conversely, glasses S3 demonstrate radiation shielding capabilities that are commensurate with those of the lead-glasses exhibiting 45% mole concentrations. This observation suggests that the newly developed glasses possess commendable radiation shielding properties, thereby establishing them as viable candidates for applications in the domain of radiation protection.

An exceptional enhancement in the attenuation efficacy of the proposed S6 glass was observed with the integration of the extracted Pb and Bi elements. This phenomenon is clearly manifested in the behavior of half-value layers , as illustrated in Figure 6. From a shielding standpoint, ascertaining the requisite thickness of the shield to mitigate radiation intensity to a permissible threshold is of paramount importance. Materials must exhibit a low HVL value to effectively function as a shielding agent. In Figure 6, various energy levels have been scrutinized to analyze the effect of Bi_2O_3 concentration on HVL. The data presented in Figure 6 indicate that the correlation between

HVL and Bi_2O_3 concentration is of an inverse nature. HVL diminishes with the incremental addition of Bi_2O_3 to the glass matrix.

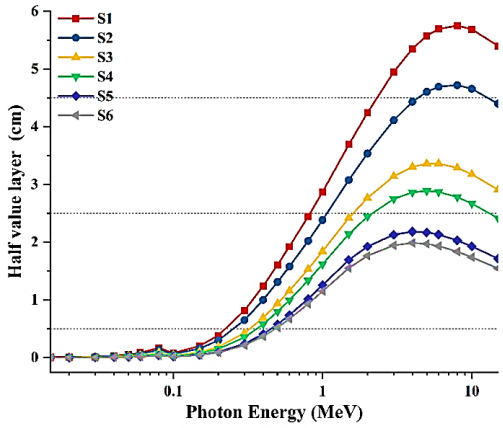

Figure 6. The half-value layer for the S1 to S6 selected glass samples

This trend implies that an increase in Bi_2O_3 concentration augments the photon shielding effectiveness of the S6 glass. Quantitative data can elucidate this observation. For this analysis, the Bi_2O_3-free glass (S2) and the glasses containing 50 and 55 mol% (S5 and S6) were selected. HVL is observed to decrease from 5.69 cm for S1 to 1.93 cm for S6 at 6 MeV, from 1.6 to 0.52 cm at 0.5 MeV, and from 0.2 to 0.044 cm at an energy level of 0.15 MeV. Furthermore, Figure 6 clearly demonstrates that HVL is a characteristic dependent on energy levels. At 5 MeV, the highest HVL values for all samples are evident. Consequently, it may be recommended that thicker material be employed to obstruct high-energy radiation.

The HVL values illustrated in Figure 7 demonstrate an upward trajectory across all specimens as gamma energy escalates. This increase in HVL is ascribed to the inverse correlation between HVL and LAC values. Furthermore, to evaluate the efficacy of the selected glass materials, the HVL values were compared with those obtained from antecedent studies involving tungsten and lead glasses [39, 40].

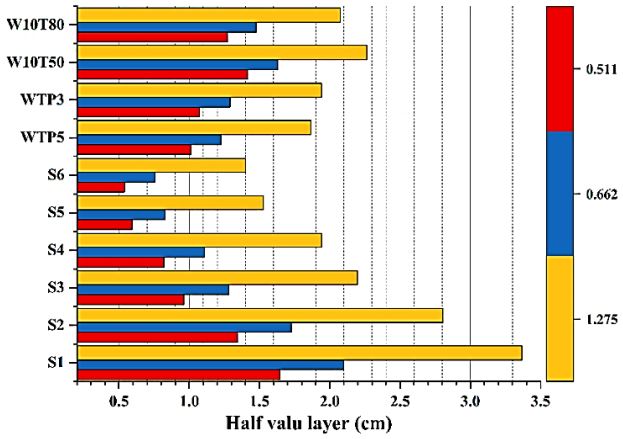

Figure 7. Comparison of half-value layer for the selected glass samples

As shown in Figure 7, the values are relatively similar in a significant part of the energy spectrum, especially at the energy level of 0.511 MeV, which indicates that the investigated samples showed lower thickness compared to the previously established criteria. Importantly, the investigated glass samples showed consistency with samples containing effective absorbing such as lead and tungsten. With increasing energy level, the difference in thickness between the current samples and the samples of previous studies decreased, indicating an increase in the performance of the samples at higher energies. As a result, the acceptable effect of the selected samples was evident not only at lower energy but also at higher energy thresholds.

Figure 8 illustrates the plot of the TVL. Prior to the analysis of this figure, it is imperative to acknowledge that a reduced TVL is recommended for an enhanced protective medium to minimize the requisite thickness aimed at decreasing radiation levels to permissible limits. Given the multitude of interactions occurring between the incident photon and the absorber, there exists a propensity for augmented attenuation and enhanced shielding characteristics. As energy levels increase, there is a concomitant rise in the TVL. The minimum TVL recorded for selected glass samples at an energy level of 8 MeV are 19.11 cm and 6.1 cm for samples S1 through S6, respectively. For sample S5, the maximum TVL is measured at 7.1 cm. The addition of Bi_2O_3 resulted in a decrease in TVL, with S6 showing the lowest TVL and superior performance over the others. This phenomenon can be attributed to the density of the medium, as the increment of 5% mol of Bi_2O_3 elevates its density from 7.8 to 8.49 g/cm³, thereby enhancing the medium's capability to shield against photons through increased interaction with a greater number of photons. Due to its maximum density compared to the other glass samples, S6 (density=7.8 g/cm^3) exhibited the most effective photon attenuation properties. This observation indicated that photon-matter interactions were enhanced for samples with higher Bi_2O_3 concentrations (i.e., higher densities) across the entire energy spectrum. The results presented in Figure 8 showed that as the photon energy increased, the effectiveness of the glasses in attenuating photons decreased, thus facilitating the passage of photons through glass samples S1 to S6 more easily.

For all specimens categorized from S1 to S6, within the delineated photon energy spectrum ranging from 0.015 to 10 MeV, the fluctuations in the effective atomic number, are meticulously illustrated in Figure 9. In this framework (as depicted in Figure 9), it is imperative to acknowledge that the Z_{eff} values demonstrate a correlation with both the photon energy levels, which exhibit a congruent trend throughout the spectrum, and the chemical composition of the analyzed glass materials. Materials characterized by a higher effective atomic number are typically associated with an augmented number of atomic constituents, which consequently increases the probability of interactions

between incident photons and the atomic matrix, thereby resulting in enhanced photon attenuation. Among the entire range of S1 to S6 samples under scrutiny, it is discerned that glass sample S6 reveals the maximum Z_{eff} values, attributable to its comparatively elevated concentration of elements with high atomic numbers, such as Bismuth (Bi).

It is noteworthy that the Z_{eff} values for all scrutinized samples are relatively greater at lower photon energy levels, particularly within the interval of 0.015 to 0.2 MeV, and subsequently exhibit a rapid decline up to the energy threshold of 1 MeV, followed by a sharp increment observed at 100 KeV, which can be ascribed to the K-edge absorption phenomena of elements such as lead and Bismuth, since the photoelectric absorption phenomenon, which is proportional to Z raised to the power of 4.5, governs this specific energy domain.

Progressing further, across the photon energy spectrum from 0.2 to 1.5 MeV, for all samples designated as S1 to S6, the effective atomic number, Z_{eff}, attains a nadir due to the prevailing influence of the CS mechanism, which is directly proportional to Z, within this intermediate energy range. With subsequent increases in the photon energy spectrum, from 1.5 to 10 MeV, there is a systematic augmentation of Z_{eff} values across all glass samples, which can be attributed to the predominance of Pair Production (PP) phenomena, which is proportional to Z squared, occurring within the nuclear domain. To exemplify, the derived effective atomic number values at specific photon energy levels of 2 and 15 MeV further corroborate this observation. Given that sample S6 exhibits the highest Z_{eff} values among all analyzed glass specimens, it is conjectured to be the most advantageous selection for effective photon attenuation.

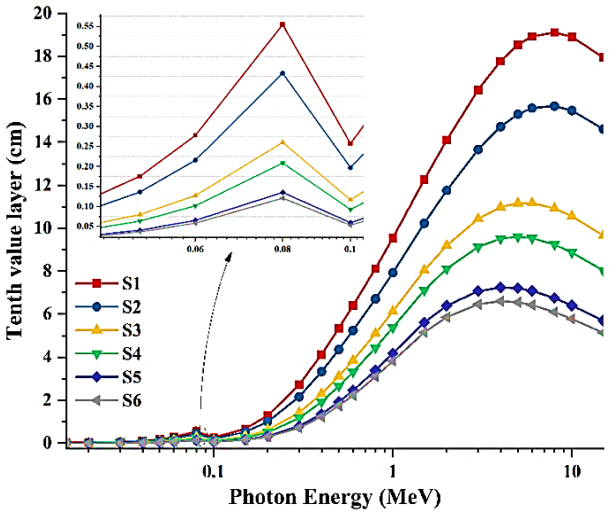

Figure 8. The tenth-value layer for the S1 to S6 selected glass samples

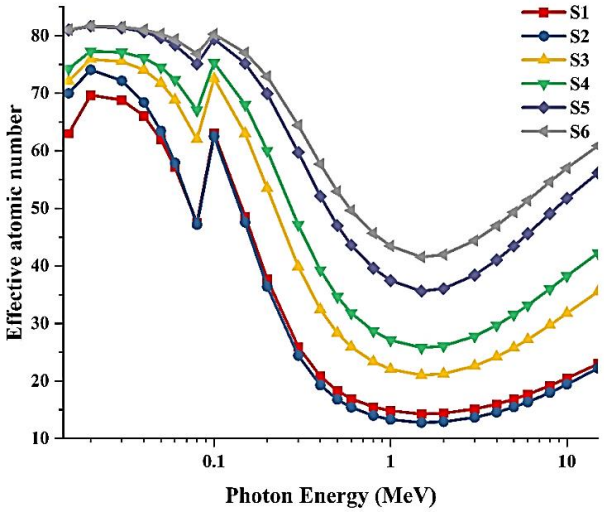

Figure 9. The effective atomic number for the S1 to S6 selected glass samples

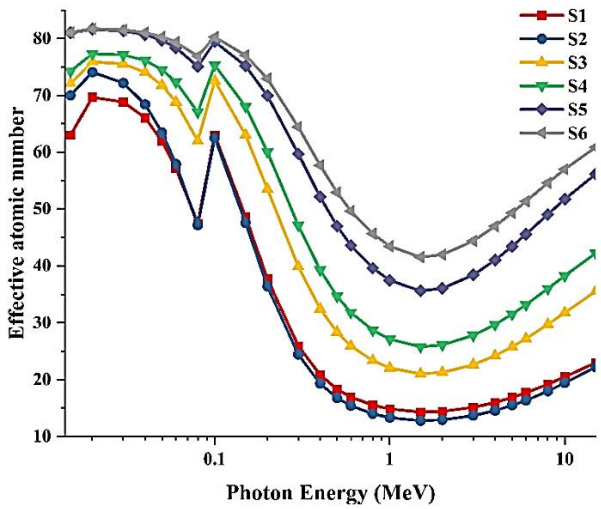

Figure 10. The effective electron density for the S1 to S6 selected glass samples

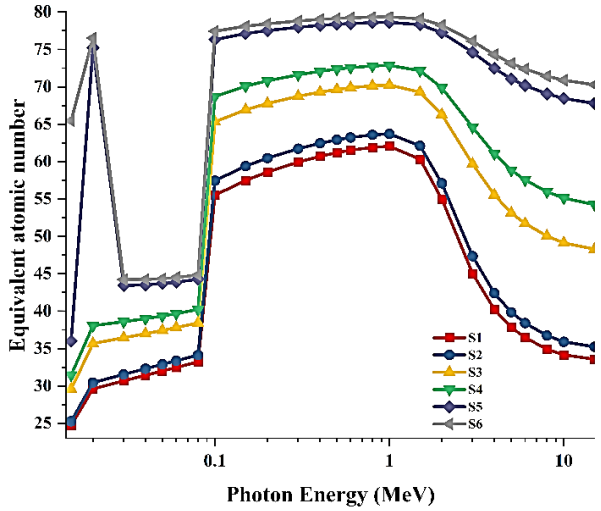

Figure 11. The equal atomic number for the S1 to S6 selected glass samples

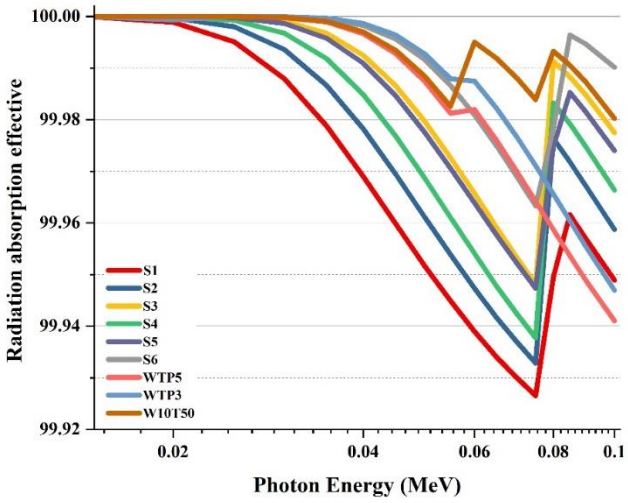

Figure 12. Comparison radiation absorption effective for the selected glass samples

Figure 10 provides an exhaustive illustration of the variations in the effective electron number across the photon energy spectrum ranging from 0.015 to 10 MeV for all samples labeled S1 through S6. In this analysis, the trend observed in N_{eff} values at each specified photon energy level exhibits a close correlation with the Z_{eff} parameters across all samples and can be elucidated in a manner akin to the Z_{eff} analysis, considering the effects of the respective interaction of photoelectric absorption, Compton scattering, and pair production at lower, intermediate, and higher energy levels, respectively. However, it is crucial to emphasize that, in contrast to the behavior demonstrated by Z_{eff}, the variances in N_{eff} values among all samples do not exhibit substantial fluctuations with an increase in photon energy, spanning from 15 keV to 10 MeV. Both the effective atomic number, Z_{eff}, and the effective electron number, N_{eff}, are critical parameters in assessing a material's potential effectiveness in providing shielding against photon radiation. Generally, an elevated N_{eff} value signifies an augmentation in the interactions between photons and electrons, as well as an escalation in the likelihood of energy transfer occurring within the material.

The equivalent atomic number serves as a fundamental concept employed in investigations regarding X-ray and gamma-ray attenuation to elucidate the interaction of photons with a material as if it were composed of a singular element. A material possessing the highest Z_{eq} will attenuate low-energy photons to the utmost degree. Figure 11 illustrates the Z_{eq} as a function of photon energy for six distinct HMO glass specimens. The Z_{eq} of all six HMO glass specimens diminishes as the photon energy increases. This phenomenon occurs because higher-energy photons are inherently more likely to traverse the material without engaging in interaction. Sample S6 exhibited a superior Z_{eq} value among all six specimens across the entire range of photon energies. This finding indicates that S6 functions as a more effective material for radiation attenuation concerning low-energy photons. The Z_{eq} values for sample S1 are comparatively lower, suggesting that these six materials exhibit similar characteristics in photon attenuation. It was further observed that the equivalent atomic number of HMO glasses is dependent upon their chemical composition.

Figure 12 illustrates the radiation absorption efficiency of selected glasses labeled S1–S6 along with selected reference glasses, across photon energies ranging from approximately 0.01 to 0.1 MeV. All materials exhibit an overall decline in shielding performance as photon energy increases, a trend fully consistent with the well-established shift from photoelectric effect–dominated interactions at lower energies to Compton scattering–dominated interactions at higher energies within this range. Among the tested compositions, those incorporating high atomic number (Z) elements—particularly tungsten-containing glasses such as W10T50 and WTP3 along with S6—demonstrate the highest absorption efficiencies, maintaining values remarkably close to 100% throughout much of the energy spectrum. In contrast, sample S1 displays the poorest shielding capability, while S6 manifests a pronounced dip followed by a sharp recovery in absorption efficiency between approximately 0.07 and 0.08 MeV; this behavior is attributed to K-edge absorption effects associated with the presence of lead and bismuth in the glass matrix, whereas the K-edge of tungsten itself occurs at around 69.5 keV (0.0695 MeV). These irregular, non-monotonic features in the attenuation curves vividly underscore the critical role that atomic shell structure and elemental composition play in determining photon interaction probabilities. From the standpoint of radiation protection physics, the data highlights a crucial principle: even minute deviations from 100% absorption can have a disproportionately large impact on shielding effectiveness, as a seemingly small reduction in attenuation percentage corresponds to a significantly higher fraction of transmitted radiation dose. The findings further reveal that bismuth–lead glasses especially sample S6 exhibit attenuation performance that is either superior or comparable to that of conventional tellurite-based formulations, particularly within the diagnostic medical energy range (approximately 0.015 to 0.1 MeV), where the photoelectric effect dominates and the high-Z constituents (such as Bi and Pb) exert their maximum influence on photon absorption. Consequently, the optimal selection of shielding materials must consider not only their average attenuation capacity but also the detailed spectral profile of the radiation source to be mitigated. While high-Z composite materials generally provide more stable and reliable protection across a broad energy interval, those exhibiting sharp K-edge features may offer strategic advantages—or pose unexpected vulnerabilities—depending on whether the operational photon energies align with or fall near these absorption thresholds. This nuanced understanding strongly supports the development and deployment of customized, compositionally engineered shielding solutions designed to minimize performance gaps near critical absorption edges and to ensure robust, energy-resilient protection against diverse photon fields encountered in medical, industrial, and research settings.

It is imperative to emphasize that materials utilized for radiation attenuation are not distinguished by a slender morphology, and the emanated gamma-ray emissions are broad and fail to adhere to the Lambert-Beer law. In this framework, a corrective parameter known as the buildup factor (BF) is incorporated into the intensity equation. The energy spectrum spanning from 0.015 to 10 MeV up to 40 mfp penetration depths for the chosen glass specimens has been scrupulously computed. The Geometrical Progression method has been developed for the determination of buildup factors. Typically, reduced values of the Equivalent Buildup Factor and Equivalent Absorption Buildup Factor for a specific material correlate with a diminished probability of gamma-ray penetration through it. At penetration depths of 1, 5, 10, 15, 20, 25, 30, 35, and 40 mfp, the calculated EBF and EABF values demonstrate variations across the gamma-ray energy spectrum of 0.015

to 10 MeV for all samples S1 through S6, as depicted in the collections presented in Figure 13 and Figure 14, respectively. Within the photon energy spectrum ranging from 0.015 to 10 MeV, the calculated equivalent atomic numbers (Z_{eq}) and G-P fitting parameters for the estimation of EBF and EABF have been utilized [41]. It is noteworthy that analogous patterns in the alteration of EBF and EABF values are discerned across the entire spectrum of photon energies for the designated glass samples. In the energy interval extending from 0.5 to 10 MeV, both EBFs and EABFs demonstrate minimal values with inconsequential fluctuations, notwithstanding sporadic abrupt increases observed at photon energies between 0.015 to 0.15 MeV, which can be attributed to the respective L1 and K-edges absorption of Lead (Pb) and Bismuth (Bi) elements, at specific mean free path (mfp) penetration depths of 1, 5, 10, 15, 20, 25, 30, 35, and 40. Predominantly, the PE effect is the primary interaction mechanism in this lower energy domain (up to 150 keV).

Subsequently, as the energy escalates from 0.02 to 5 MeV (and even extends to 2 MeV at increased penetration depths), both EBFs and EABFs portray a gradual augmentation, respectively, attributable to the dominance of the CS phenomenon (characterized by multiple photon scatterings with minimal energy reduction followed by subsequent PE absorption) within this intermediate energy domain for all samples designated as S1 to S6. As a result, with the prolongation of the photon's lifetime, the likelihood of its escape through the sample is significantly enhanced. Typically, the CS process is predominant within the energy spectrum of 250 keV to 3 MeV. Furthermore, predicated upon the chemical composition of the glasses (samples S1 to S6), from 6 or 3 to 10 MeV energies, both EBFs and EABFs are observed to be elevated due to the influence of the Pair Production process at these elevated gamma-ray energy levels. It is well-documented that a photon possessing an energy threshold of at least 1.022 MeV can generate an electron-positron pair. Moreover, for all analyzed samples, EBFs and EABFs are noted to be enhanced in correlation with the sample's mfp values, commencing from 5 mfp.

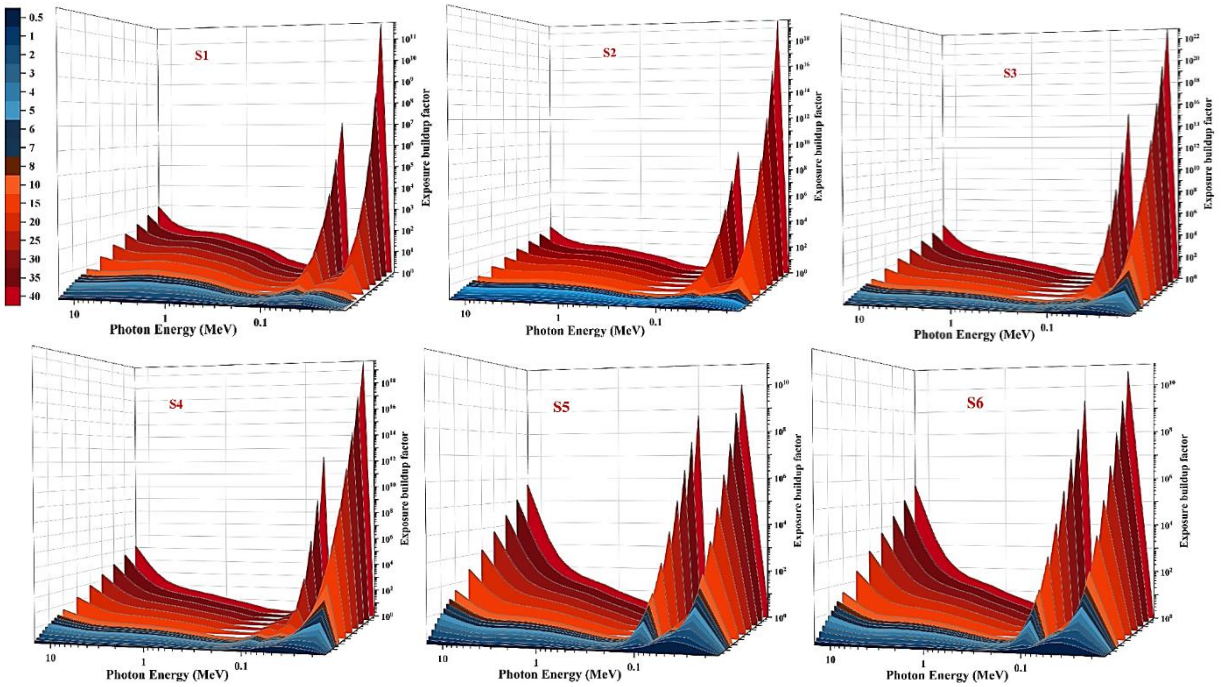

Figure 13. Variation of exposure buildup factor with photon energy at different mean free paths for the S1 - S6 selected glass samples

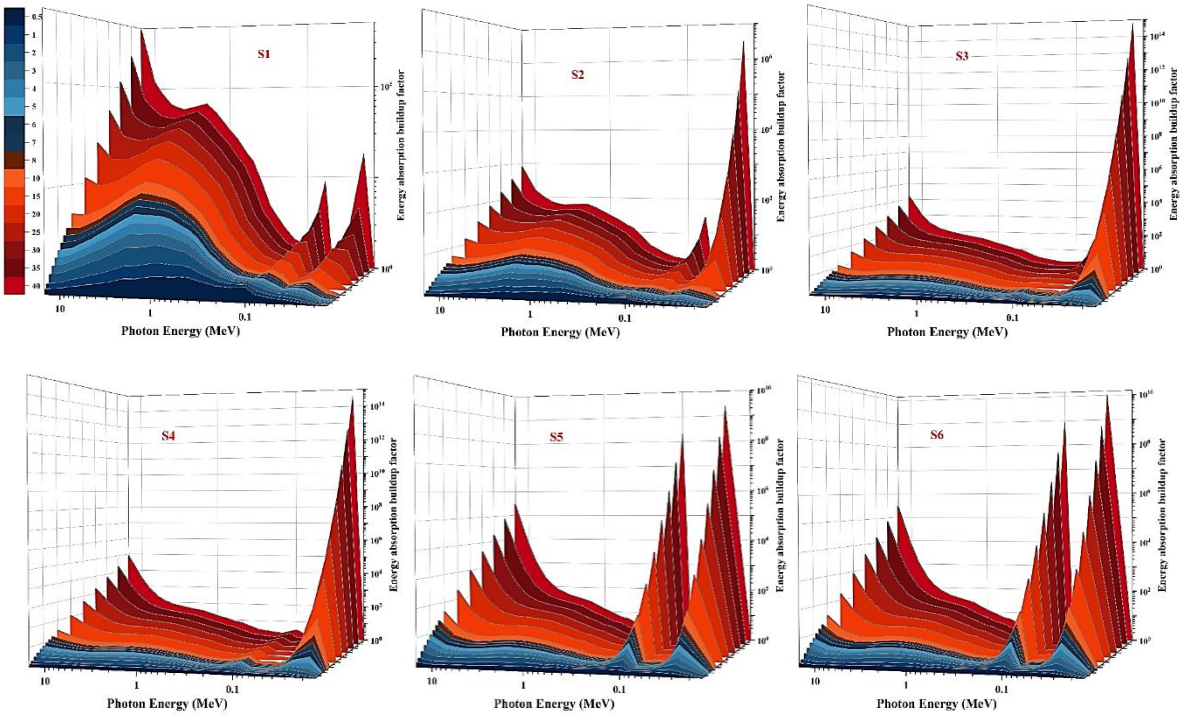

Figure 14 . Variation of energy absorption buildup factor with photon energy at different mean free paths for all S1-S6 selected glass samples

At elevated energies (and correspondingly, at increased penetration depths), secondary photons resulting from the annihilation of positrons and electrons (culminating in the generation of two gamma-rays each possessing an energy of 0.511 MeV) are scattered with greater frequency, thereby leading to a substantial accumulation of photons. The resultant two gamma-ray photons are capable of either escaping or interacting with the sample through the mechanisms of CS or the PE effect. An escalation in atomic number is associated with an increase in the atomic cross-section pertinent to the specific PE effect, CS, and PP mechanisms. Due to the augmented ratio of Z_{eq} to Z_{eff}, among the samples coded from S1 to S6, the glass sample identified as S6 displays diminished EBFs and EABFs, thereby signifying its enhanced efficacy as a gamma-ray shielding material. Figure 15 delineates the values of the fast neutron removal cross-section for six distinct glass compositions, in comparison with commonly employed materials such as water, boron carbide, paraffin and concrete, thereby facilitating a thorough comparative examination of their respective shielding efficiencies. The results reveal that the glass specimen labeled as S2 demonstrates the highest neutron removal cross-section, quantified at approximately 0.1229 cm^{-1}, which is slightly superior to that of paraffin, recorded at 0.121 cm^{-1}, thereby illustrating a significant performance advantage. In stark contrast, conventional shielding materials, including water, paraffin, and concrete, display relatively inferior neutron removal cross-section values, with concrete exhibiting the lowest effectiveness, measured at approximately 0.085 cm^{-1}, thereby highlighting its limitations in neutron attenuation [42].

This data implies that the glass material S2 has the potential to serve as a considerably more effective neutron shielding alternative to traditional materials, thereby offering enhanced protective measures in environments characterized by high fast neutron fluxes, which are prevalent in various nuclear and radiological contexts.

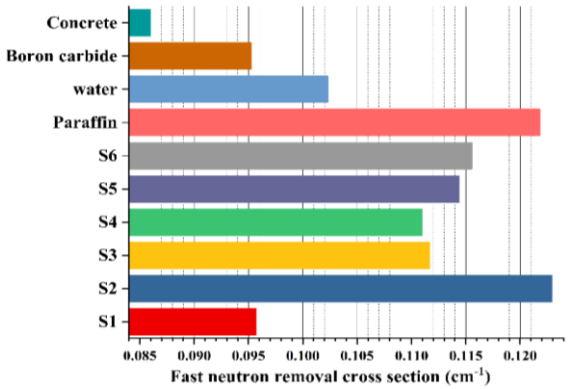

Figure 15. The effective neutron removal cross-section for all S1-S6 selected glass systems

Discussion

The investigation into PbO-Al_2O_3-B_2O_3-SiO_2-Bi_2O_3 glasses revealed a direct correlation between heavy metal oxide content, structural properties, and gamma-ray shielding performance. The density of the glasses increased significantly with HMO concentration, ranging from 3.61 to 8.50 g/cm^3, with Bi_2O^3

demonstrating a more pronounced effect on densification and molar volume expansion than PbO. Radiation shielding parameters were rigorously validated, showing excellent agreement between Geant4 simulations and Phy-X/PSD theoretical calculations, with relative differences below 2%. Critically, the mass attenuation coefficient and linear attenuation coefficient were enhanced by higher Bi_2O_3 content, with sample S6 (55 mol% Bi_2O_3) consistently exhibiting the highest values. Its LAC at 0.662 MeV (0.9186 cm^{-1}) surpassed that of conventional lead-based glasses. This superior attenuation is reflected in lower half-value layer and tenth-value layer thicknesses for Bi_2O_3-rich glasses; for instance, the HVL of S6 was reduced to 1.93 cm at 6 MeV, compared to 5.69 cm for the Bi_2O_3-free sample S1. The effective atomic number and equivalent atomic number analyses confirmed that S6, with the highest values, is the most effective composition for photon attenuation, particularly at lower energies where the photoelectric effect dominates, as evidenced by K-edge absorption features. Furthermore, the glass compositions demonstrated favorable buildup factors and, notably, sample S2 exhibited a high fast neutron removal cross-section (0.1229 cm^{-1}), exceeding that of paraffin. In conclusion, the systematic incorporation of Bi_2O_3, more so than PbO, optimally enhances photon and neutron attenuation, positioning these HMO glasses, particularly the Bi_2O_3-rich S6 composition, as highly effective candidates for advanced radiation shielding applications.

Conclusion

This study evaluated the gamma- and neutron-shielding performance of PbO–Al_2O_3–B_2O_3–SiO_2 glasses with increasing Bi_2O_3 content (samples S1–S6). The outcomes demonstrate that sample S6—containing the greatest Bi_2O_3 concentration—exhibits superior gamma-ray attenuation, particularly in the diagnostic medical energy range (15–100 keV). At 30 keV, for instance, S6 achieves near-complete absorption (>99%), whereas S1—the lowest-Bi_2O_3 sample—shows significantly reduced shielding efficiency. This enhancement is attributed to the high atomic numbers of Bi (Z = 83) and Pb (Z = 82), which maximize photoelectric absorption at low energy levels. A distinct dip in S6's absorption curve near 90.52 keV corresponds to the K-edge of bismuth, confirming the strong influence of elemental structure on photon interactions. Quantitatively, S6 displays the lowest HVL and TVL across the 0.015–0.1 MeV range, outperforming not only S1–S5 but also several conventional tellurite-based shielding glasses. S6 is unequivocally the most effective gamma shield among the selected compositions. For neutron shielding, S2 shows the highest fast neutron removal cross-section (0.1229 cm^{-1}), slightly exceeding paraffin (0.121 cm^{-1}) and significantly surpassing concrete (0.085 cm^{-1}), suggesting its potential in mixed-field environments. Given S6 exceptional performance in the diagnostic energy range is highly suitable for radiation protection in medical settings such as X-ray room windows, and syringe shields in nuclear medicine—where lightweight, non-toxic, and high-efficiency materials are urgently needed. Future work should focus on optimizing Bi_2O_3–PbO ratios to smooth K-edge discontinuities and exploring composite laminates that integrate S6 for gamma shielding with hydrogen-rich layers (e.g., S2-inspired matrices) for neutron attenuation, enabling tailored solutions for radiotherapy center, PET/CT facilities, and portable radiography units.

References

1. Jain S. Radiation in medical practice & health effects of radiation: rationale, risks, and rewards. J Family Med Prim Care. 2021;10(4):1520.
2. Subedi B, Paudel J, Lamichhane TR. Gamma-ray, fast neutron and ion shielding characteristics of low-density and high-entropy Mg–Al–Ti–V–Cr–Fe–Zr–Nb alloy systems using Phy-X/PSD and SRIM programs. Heliyon. 2023;9(7):e17725.
3. ALMisned G, Elshami W, Issa SA, Süsoy G, Zakaly HM, Algethami M, et al. Enhancement of gamma-ray shielding properties in cobalt-doped heavy metal borate glasses: the role of lanthanum oxide reinforcement. Materials. 2021;14(24):7703.
4. Al-Buriahi MS, El-Agawany FI, Sriwunkum C, Akyıldırım H, Arslan H, Tonguç BT, et al. Influence of Bi_2O_3/PbO on nuclear shielding characteristics of lead-zinc-tellurite glasses. Physica B. 2020;581:411946.
5. Kaky KM, Sayyed MI. Selected germanate glass systems with robust physical features for radiation protection material use. Radiat Phys Chem. 2024;215:111321.
6. Alzahrani JS, Alrowaili ZA, Saleh HH, Hammoud A, Alomairy S, Sriwunkum C, et al. Synthesis, physical and nuclear shielding properties of novel Pb–Al alloys. Prog Nucl Energy. 2021;142:103992.
7. Hiremath GB, Hosamani MM, Vinayak A, Patil PN, Singh VP, Ayachit NH, et al. Investigation of gamma ray, electron, and neutron interaction parameters of some topological insulating materials. Radiat Eff Defects Solids. 2022;178(3-4):335-51.
8. Saeed A, Alomairy S, Sriwunkum C, Al-Buriahi MS. Neutron and charged particle attenuation properties of volcanic rocks. Radiat Phys Chem. 2021;184:109454.
9. Ahmadi M, VahidZanganeh V, DarushNaderi N. Investigated mechanical, physical parameters and gamma-neutron radiation shielding of the rare earth (Er_2O_3/CeO_2) doped barium borate glass: role of melting time and temperature. Radiat Phys Chem. 2024;217:111450.
10. Alzahrani JS, Alrowaili ZA, Olarinoye IO, Katubi KM, Al-Buriahi MS. Effect of ZnO on radiation shielding performance and gamma dose of boron silicate glasses. Silicon. 2023;16(1):105-13.
11. Katubi KM, Olarinoye IO, Alrowaili ZA, Al-Buriahi MS. Optical transmission, polarizability, and photon/neutron shielding properties of Bi_2O_3/MnO/B_2O_3 glass system. Optik. 2022;268:169695.
12. Sayyed MI, Al-Hadeethi Y, Alshammari M, Ahmed M, Al-Heniti S, Rammah YS. Physical, optical and gamma radiation shielding competence of newly

boro-tellurite based glasses: TeO_2–B_2O_3–ZnO–Li_2O_3–Bi_2O_3. Ceram Int. 2021;47(1):611-8.
13. Sekhar KC, Ahmed MR, Narsimlu N, Deshpande U, Sathe V, Shareefuddin M. The effect of the addition of CaF_2 and PbF_2 on boro-tellurite glasses doped with chromium ions. Mater Res Express. 2020;6(12):125206.
14. Sayyed MI, Sadeq MS, Shaaban KS, El-Rehim AFA, Ali AM, Morshidy H. Elucidating the effect of La_2O_3–B_2O_3 exchange on structure, optical and radiation shielding improvements of Na_2O–NiO–B2O3 glass. Opt Mater. 2023;142:114051.
15. Shaaban KS, Althagafi TM, Ashour A, Alalawi A, Al-Buriahi MS, Ibraheem AA. The role of Nb_2O_5 on structural, mechanical, and gamma-ray shielding characteristics of lithium molybdenum borate glasses. Radiat Phys Chem. 2024;216:111440.
16. El-Rehim AFA, Zahran HY, Yahia IS, Wahab EAA, Shaaban KS. Structural, elastic moduli, and radiation shielding of SiO_2-TiO_2-La_2O_3-Na_2O glasses containing Y_2O_3. J Mater Eng Perform. 2021;30(3):1872-84.
17. Shaaban KS, Alomairy S, Al-Buriahi MS. Optical, thermal and radiation shielding properties of B_2O_3–NaF–PbO–BaO–La_2O_3 glasses. J Mater Sci Mater Electron. 2021;32(21):26034-48.
18. Shaaban KS, Tamam N, Alghasham H, Alrowaili ZA, Al-Buriahi MS, Ellakwa TE. Thermal, optical, and radiation shielding capacity of B_2O_3-MoO_3-Li_2O- Nb_2O_5 glasses. Mater Today Commun. 2023;37:107325.
19. Shaaban KS, Al-Baradi AM, Ali AM. Investigation of BaO reinforced TiO_2–P_2O_5–Li_2O glasses for optical and neutron shielding applications. RSC Adv. 2022;12(5):3036-43.
20. Althagafi TM, Sayed MA, Alghasham H, Al-Harbi N, Shaaban KS. The impact of changing the LiF concentration on structural, thermal, physical, and optical properties of CdO—SiO_2—B_2O_3—MoO_3—LiF glasses. Silicon. 2023;15(16):7047-56.
21. Al-Baradi AM, Wahab EAA, Shaaban KS. Preparation and characteristics of B_2O_3–SiO_2–Bi_2O_3–TiO_2–Y_2O_3 glasses and glass-ceramics. Silicon. 2021;14(10):5277-87.
22. Shaaban KS, Al-Baradi AM, Ali AM. The impact of Cr2O3 on the mechanical, physical, and radiation shielding characteristics of $Na_2B_4O_7$–CaO–SiO_2 glasses. Silicon. 2022;14(16):10375-82.
23. Koubisy MSI, Shaaban KS, Wahab EAA, Sayyed MI, Mahmoud KA. Synthesis, structure, mechanical and radiation shielding features of 50SiO_2–(48+X) $Na_2B_4O_7$-(2−X) MnO_2 glasses. Eur Phys J Plus. 2021;136(2):197.
24. Shaaban KS, Alotaibi BM, Youf ES. Effect of La_2O_3 concentration on the structural, optical and radiation-shielding behaviors of titanate borosilicate glasses. J Electron Mater. 2023;52(6):3591-603.
25. Alyousef HA, Alrowaili ZA, Saad M, Almohiy HM, Alshihri AA, Shaaban KS, et al. Examinations of mechanical and shielding properties of CeO_2 reinforced B_2O_3–ZnF_2–Er_2O_3–ZnO glasses for gamma-ray shield and neutron applications. Heliyon. 2023;9(3):e14435.
26. Park J, Kim HJ, Kim S, Cheon J, Kaewkhao J, Limsuwan P, et al. X-ray and proton luminescences of bismuth-borate glasses. J Korean Phys Soc. 2011;59(2):657-60.
27. Thakur V, Thakur V, Kaur A, Singh L. Synthesis and the study of structural, thermal and optical properties of (100-x) Bi_2O_3-x(BaO-TiO_2) glass system. Optik. 2020;223:165646.
28. Alomairy S, Alrowaili ZA, Kebaïli I, Wahab EAA, Mutuwong C, Al-Buriahi MS, et al. Synthesis of Pb_3O_4-SiO_2-ZnO-WO_3 glasses and their fundamental properties for gamma shielding applications. Silicon. 2021;14(10):5661-71.
29. Fayad AM, Shaaban KS, Abd-Allah WM, Ouis MA. Structural and optical study of CoO doping in borophosphate host glass and effect of gamma irradiation. J Inorg Organomet Polym Mater. 2020;30(12):5042-52.
30. Albarzan B, Almuqrin AH, Koubisy MSI, Wahab EAA, Mahmoud KA, Sayyed MI. Effect of Fe_2O_3 doping on structural, FTIR and radiation shielding characteristics of aluminium-lead-borate glasses. Prog Nucl Energy. 2021;141:103931.
31. Waly MA, El-Sayed AWA, Al-Qous GS, Bourham MA. Shielding properties of glasses with different heavy elements additives for radiation shielding in the energy range 15–300 keV. Radiat Phys Chem. 2018;150:120-4.
32. Alipoor MR, Eshghi M. Nickel/multiwalled carbon nanotube composites as gamma-ray shielding. Nano. 2024;19(6):2450027.
33. Zou C, Luan G, Luo H, Zhang Q, Ren J, Ruan X, et al. Geant4 simulation of the gamma-ray total absorption facility. Symmetry. 2025;17(1):92.
34. El-Khayatt AM. Calculation of gamma-ray attenuation parameters for local rocks. Radiat Phys Chem. 2019;165:108496.
35. Alipoor MR. Enhancing gamma-ray shielding performance of HDPE composites using PbO and Bi_2O_3 reinforcements. J Korean Phys Soc. 2025;87:243-53.
36. Alajerami YS, Mhareb MHA, Sayyed MI, Al-Ghamdi H, Almuqrin AH, Alshahri F, et al. Comprehensive study for radiation shielding characteristics for Bi_2O_3-B_2O_3–ZnO composite using computational radioanalytical Phy-X/PSD, MCNP5, and SRIM software. Sci Rep. 2025;15(1):4527.
37. Alipoor MR, Eshghi M, Sever R. Monte Carlo simulation of gamma and neutron shielding with high-performance ultra-heavy cement composite. J Med Phys. 2024;49(4):661-72.
38. Issa SAM. Effective atomic number and mass attenuation coefficient of PbO–BaO–B_2O_3 glass system. Radiat Phys Chem. 2015;120:33-7.
39. Gaikwad DK, Obaid SS, Sayyed MI, Bhosale RR, Awasarmol VV, Kumar A, et al. Comparative study of gamma ray shielding competence of WO_3-TeO_2-PbO glass system to different glasses and concretes. Mater Chem Phys. 2018;213:508-17.
40. Ersundu AE, Büyükyıldız M, Ersundu MÇ, Şakar E, Kurudirek M. The heavy metal oxide glasses within the WO_3-MoO_3-TeO_2 system to investigate the shielding properties of radiation applications. Prog Nucl Energy. 2017;104:280-7.

41. Eshghi M. Investigation of radiation protection features of the TeO_2–B_2O_3–Bi_2O_3–Na_2O–$NdCl_3$ glass systems. J Mater Sci Mater Electron. 2020;31(20):16479-97.
42. Frederick CH, Julius FM, Jecong JFM, Hila FC, Castañaga IS, Dingle CAM, et al. ENDF/B-VIII-based fast neutron removal cross sections database in Z = 1 to 92 generated via multi-layered spherical geometry. Radiat Phys Chem. 2023;206:110770.